ADVANCED MATERIALS TECHNOLOGIES
www.advmattechnol.de

Photothermoelectric AZO/SiO_2/NiO Device

Catarina Bianchi, Ana Marques, and Isabel Ferreira*

Transparent-conductive-oxide (TCO) materials and transparent devices combining photovoltage and thermoelectric effects are still scarce. Hence, a new transparent-conductive-oxide/insulating/transparent-semiconductor-oxide (TCO-I-TSO) structure combining such effects is developed. It is made of aluminum-doped zinc oxide (AZO)/SiO_2/NiO thin films sequentially deposited on glass substrates. AZO exhibits thermo and photovoltage in response to gradient temperature and absorption of UV photons, while NIR photons absorption in the NiO layer. Photovoltage appears in the plane between the AZO and NiO layer when the whole sample is irradiated with near infrared light, and it also depends on the thickness of the SiO_2 layer. This photovoltage is continuously monitored on samples placed in a glass window facing south. Throughout the day, the photovoltage varies from 0 to 300 µV proportionally to the light intensity.

1. Introduction

The transition metal oxides were applied to active UV solar cells formed by n-TiO_2 and p-CuO_x nanojunctions[1] or in high efficiency UV-reactive solar cells and high performance p-type NiO/n-type ZnO photodetectors.[2] To improve the performance of transparent photovoltaics (TPV) a MoO_3 buffer layer was introduced in Co_3O_4/TiO_2 structures,[3] however, as the percentage of UV in the solar spectrum is only 9%, these solar cells have limited applications. Alternatively, new organics photovoltaics (OPV), and molecules absorbing UV and NIR wavelengths (650–800 nm) with transmittance in the visible range over 60%, has been proposed.[4] On the contrary reflection of the NIR from the spectra to avoid the excessive heating of the solar cells, and thus to increase long-term stability, was obtained using a surface high-dielectric-coated layer working as top electrode and thermal-mirror.[5] Thermoelectric properties of transparent and conductive n-type ZnO,[6] SnO_2,[7] p-type[8] oxides, and their application to transparent thermoelectric devices of rigid[9] and flexible substrates[10,11,12] has been recently reported CuI,[13] GZO,[14] as well as ZnO and indium tin oxide (ITO) solution processed devices.[15] A lack in literature was observed related to NIR photovoltage and thermoelectric (PTE) combined effects for TCO materials/devices. This effect with UV radiation was reported[10] but for the NIR it is unexplored. Hence, this work reports the influence of NiO layer thickness on infrared light absorption and charges generation by photoexcitation in aluminum-doped zinc oxide (AZO)/SiO_2/NiO structure under solar radiation. A planar thermal gradient, driven toward AZO, is converted into a thermovoltage by the Seebeck effect since NiO absorbs NIR radiation and SiO_2 is an insulating layer to avoid charge recombination at the AZO/NiO interface.

C. Bianchi, A. Marques, I. Ferreira
CENIMAT|i3N
Department of Materials Science
School of Science and Technology
NOVA University Lisbon
Largo da Torre, Caparica 2829-516, Portugal
E-mail: cb.marques@campus.fct.unl.pt

The ORCID identification number(s) for the author(s) of this article can be found under https://doi.org/10.1002/admt.202300133

DOI: 10.1002/admt.202300133

2. Results and Discussion

The transparent photothermoelectric (TPTE) AZO/SiO_2/NiO device concept herein reported relays on the NIR absorption of the NiO layer. As such, for obtaining a large band width and absorption intensity in the NIR, the NiO thickness, postdeposition annealing temperature, and time were first optimized. **Figure 1** shows the transmittance, reflectance, and absorption measured as a function of NiO film thickness, postdeposition annealing temperature, and time. For the success of TPTE device, a high transmittance in the visible range, and absorption in the NIR of solar spectrum is required. The high transmittance of NiO layer provides transparency for window applications, while high NIR absorption promotes electron photogeneration, working as heat source for the AZO (thermoelectric layer).

As expected, the transmittance greatly decreases as NiO thickness increases. The reflectance for all samples is lower than ≈30% across the entire wavelength range, and in the infrared region it is significantly lower (5%) for thinner NiO samples nonannealed, or samples annealed at 500 °C for 2 h. The absorption is in the range of 20–40%, while slightly higher for the thickest NiO film of 50 nm in the wavelength region above 1000 nm. Therefore, annealed samples have lower transmittance and thus, higher absorption. The total absorption in 750–2200 nm range was calculated as referred in Table S1 (Supporting Information). The unannealed 50 nm thick NiO films show the highest integrated absorption but also the lowest transmittance in the visible range. Therefore, for combining high infrared absorption and

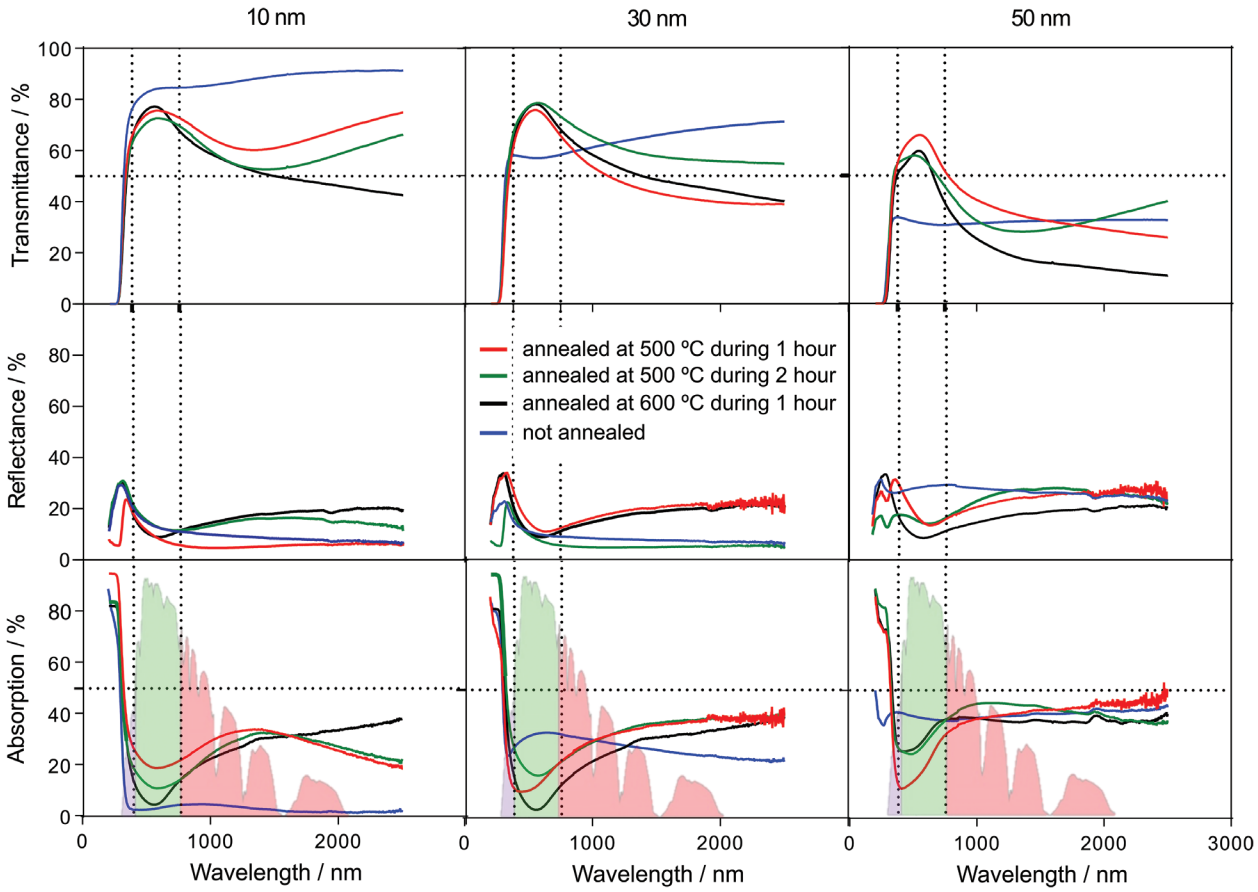

Figure 1. Transmittance, reflectance, and absorption spectra of NiO layer deposited on glass with different thicknesses and annealing temperature and time.

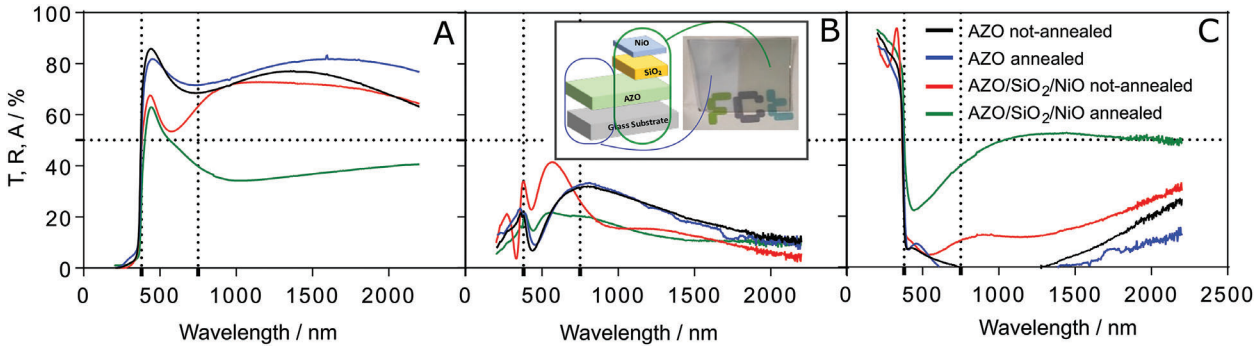

Figure 2. Transmittance A), reflectance and B) and absorption C) spectra of AZO and AZO/SiO_2/Ni device (with nonannealed and annealed at 500 °C for 1 h). A schematic and photo of the transparent photothermoelectric device is shown in (B) where AZO is shown on the left and AZO/SiO_2/NiO structure on the right.

transmission in the visible range above 50%, the 50 nm thick NiO films annealed at 500 °C for 1 h were the selected ones to produce the photothermoelectric structure (AZO/SiO_2/NiO).

As NiO is the top layer, the annealing effect on the optical properties of the AZO layer was investigated separately. **Figure 2** shows that, while the annealing step did not introduce any relevant optical modification on the AZO film, on the AZO/SiO_2/NiO structure the annealing increases the absorption in the NIR wavelengths range (λ > 1000 nm) to ≈50%, the transmittance in the visible wavelength ranges within 40–60%. Compared to self-adhesive polymeric window sunscreens on the market, this TPTE device has a good transmittance in the visible range (Figure S2, Supporting Information).

The influence of postdeposition annealing on the chemical composition and structure of the AZO and NiO layers was investigated by Raman spectroscopy. **Figure 3**A shows the Raman

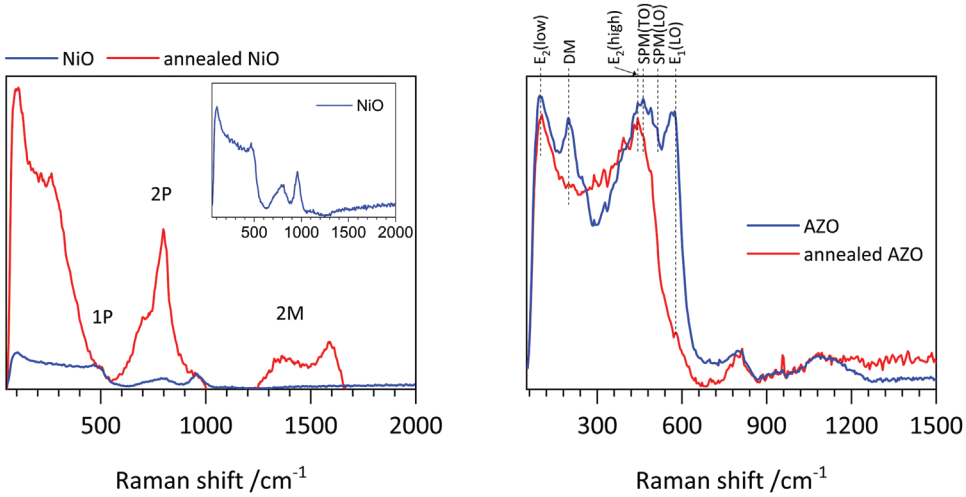

Figure 3. Raman spectra of AZO, AZO annealed, NiO and NiO annealed films deposited on glass.

spectra of AZO films before (in blue) and after annealing (in red). According to the literature,[16] peaks centered at 100, 440, and 575 cm^{-1} are assigned to active optical phonon modes. The first two peaks are doubly degenerated modes assigned to E_2(low) and E_2(high) modes, and the third peak at 575 cm^{-1} to E_1(LO) longitudinal mode. Still according to ref. [16], the E_2(high) mode is typically associated with the hexagonal ZnO Wurtzite structure, and the E_1(LO)to the O-vacancies, Zn interstitials, or a combination of both. Direct comparison with the annealed AZO spectrum reveals that it also crystallized in the hexagonal Wurtzite structure, but with better crystallinity, as the active mode peaks are sharper. Moreover, as the longitudinal and transversal surface phonon optical mode peaks (SPM(LO) and SPM(TO)) at 516 and 460 cm^{-1} almost vanished after annealing, evidence that the crystallite and grains size may have increased. This is because literature reveals that SPM modes are highly localized near the grain boundaries and are typically associated with nanocrystalline particles.[16] Also, the significant decrease of peak intensity at 575 cm^{-1} indicates a possible increase in the oxygen content of AZO film, leading to significantly less vacancies, and thus, to enhanced AZO resistivity. The peak at 193 cm^{-1} is a deformation mode (DM) that is not visible after annealing, hence, according to ref. [16] that observation may denounce that the film changed its morphology. Which is compatible with the atomic force microscopy (AFM) results shown in **Figure 4**, as after annealing, the AZO film roughness increased. Finally, the observation of the broad peak at 1101 cm^{-1} is assigned to the combination of multiphonon modes.[17,18]

Figure 3B shows the Raman spectra of NiO films before (in blue) and after annealing (in red). The peaks in both spectra are mainly attributed to magnon and optical phonon excitations as previously reported in the literature.[19] Corresponding the most prominent peaks to the one-phonon (1P) transverse optical bands, the two-phonon (2P) transverse optical bands, and to the two-magnon (2M) band as labeled in the spectra. The latter band is typically associated with NiO magnetic properties and therefore, with the material particles size. Ulmane et al. correlated the 2M-band intensity reduction with decreasing NiO nanopowders prepared by evaporation of NiO coarse grained NiO powder, and verified that the 2M band vanished when at room temperature the crystallite size attained 100 nm.[19,20,21] They attributed the decrease of the 2M-band intensity to the decrease of antiferromagnetic spin correlations. But since in Figure 3B, the 2M-peak is not visible in the spectrum acquired before annealing, it suggests that after annealing the magnetic ordering strength may have increased as well as the NiO grain size. AFM-maps shown in Figure 4A reveal that the surface roughness also increases, which might have made the NiO film more compact and with improved crystalline quality, as demonstrated by Figure 4B X-ray diffraction (XRD) diffractograms. Moreover, the two-phonon band (2P) peaks obtained in the annealed NiO film Raman spectrum are more intense and sharper. To see the variation clearly, 3B shows in the inset a zoom of the NiO blue spectrum obtained before annealing. The intensity of the 1P-TO (460 cm^{-1}) band as compared to the 2P bands in the nonannealed spectrum is higher than in the annealed NiO spectrum, where the 1P-TO band almost vanished. Being this mostly attributed to the presence of defects, or due to surface effects and imperfectness of the particles.[22] It may be also noted that the Raman spectrum of a perfect cubic and rhombohedral structured NiO does not show the peak associated to 1P longitudinal scattering (usually, centered at ≈530 cm^{-1}).[23] Hence, since such peak was not detected, it may indicate that the annealed NiO may have one of the referred structures. According to the XRD diffractograms in Figure 4B, annealed NiO might have a rhombohedral structure.

AFM surface maps of Figure 4 show higher density of grains on NiO and AZO annealed samples, and in AZO/SiO_2/NiO structures. Nevertheless, such grains are more prominent in the annealed NiO films. The Kelvin probe mapping is in concordance showing a lower surface potential of these crystalline regions. The XRD pattern of Figure 4 confirms the crystallization of NiO after annealing. As deposited NiO films show amorphous structure revealed by the absence of peaks, while after annealing a predominate peak at a 2θ angular position of 23.49° is associated to (0004) plans of phase centered orthorhombic NiO_x.[24] AFM images, Raman spectra, and XRD diffractograms (shown in Figure 4) are in concordance, and we conclude that the NIR absorption is due to a crystallization of material.

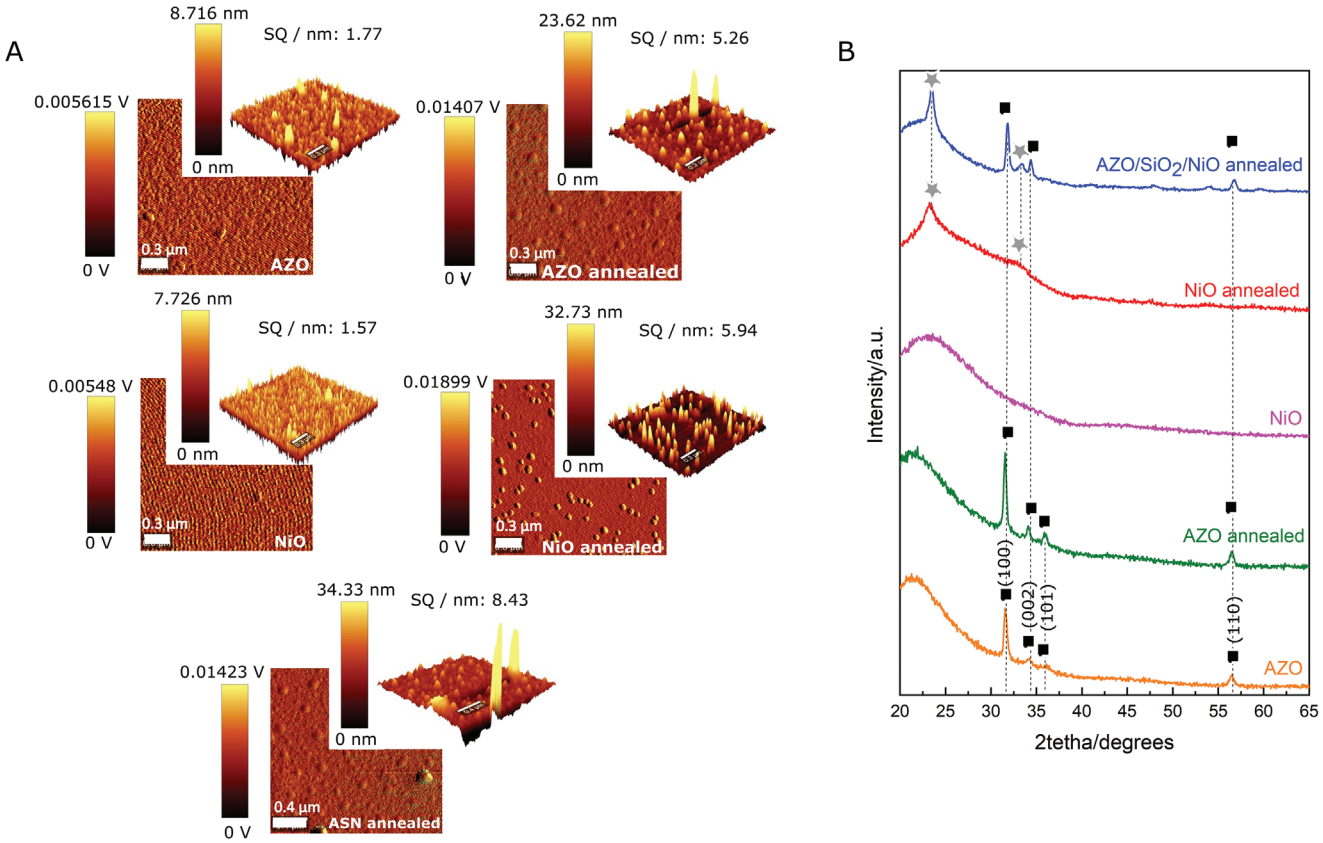

Figure 4. A) AFM maps measured on AZO, AZO annealed (both on top), NiO, NiO annealed (both at middle) and the NiO top layer of the final structure (AZO/SiO_2/NiO annealed, at bottom)—ASN annealed. B) XRD diffractograms of AZO, AZO annealed, NiO, NiO annealed and the final structure (AZO/SiO_2/NiO annealed).

The thermoelectric effect was measured as sketched in **Figure 5**A. The gradient temperature (around 2–9 °C) is established vertically, between the Peltier heat source and the room temperature, being the temperature gradient measured between the glass in contact with Peltier and NiO top film. A n-type Seebeck coefficient is obtained, −305 µV K^{-1}. The main characteristics of the layers that formed the AZO/SiO_2/NiO structure are referred in Table S2 (Supporting Information). The conductivity of both AZO and NiO are in the range of 4–6 × 10^2 S cm^{-1}, although the carrier concentration is one order of magnitude higher for AZO, attaining 10^{21} cm^{-3}. The thermoelectric voltage of NiO is very low compared to that of AZO (−15 vs −103 µV K^{-1}) due to a lower carrier concentration of NiO and both materials reveal to be n-type (Table S2, Supporting Information).

The NiO absorption of NIR radiation and photogeneration was confirmed upon irradiating the whole sample with an IR lamp. As a result, the potential (V_{OC}) increased (Figure 5B). To understand the time response and the contribution of each sample part in the structure, the voltage was continuously monitored while irradiating the whole sample, or part, by covering either AZO or NiO side with a cork sheet (Figure 5B). Covering NiO layer, the voltage signal leads to a thermoelectric effect, as the heat radiation from the lamp creates a temperature difference between AZO (hot side) and NiO (cool side), 1 mV signal is reached in about 40 s, tending to stabilize during irradiation. Switching OFF the lamp led to a signal decrease as fast as the rising time. The obtained voltage for the whole radiated sample is due to NIR absorption of NiO layer (as the whole sample is at same temperature). Covering the AZO side, leads to the cooling of the AZO layer, and the voltage signal is due to NiO absorption and to the AZO thermoelectric effect. This is confirmed by adding the curve corresponding to the total illumination of the sample (IR absorption effect) to the one obtained when the NiO film is covered (thermal effect). The values resulting from the sum are close to that obtained for the covered AZO curve (IR absorption effect + thermal effect) (Dashed line—Figure 5B). Considering the peak emission of the infrared lamp used and the different percentages of transmission, reflection, and absorption for a specific wavelength range (Table S3, Supporting Information), AZO/SiO_2/NiO can absorb a total ≈7241 nm Wm^{-2} of the solar spectrum (Table S1, Supporting Information), which clearly justifies the photothermal effect observed.

Figure 6 confirms the photogeneration by sunlight absorption, that surpassed the value of thermoelectric effect with a 9 °C thermal gradient between AZO and NiO part of AZO/SiO_2/NiO structure. The IR radiation alone also represent a great effect but when a thermal gradient and infrared light are simultaneously applied on sample, the power output is lower because the flow of carriers is opposite to that generated by the light, which reduces the number of carriers reaching the electrodes.

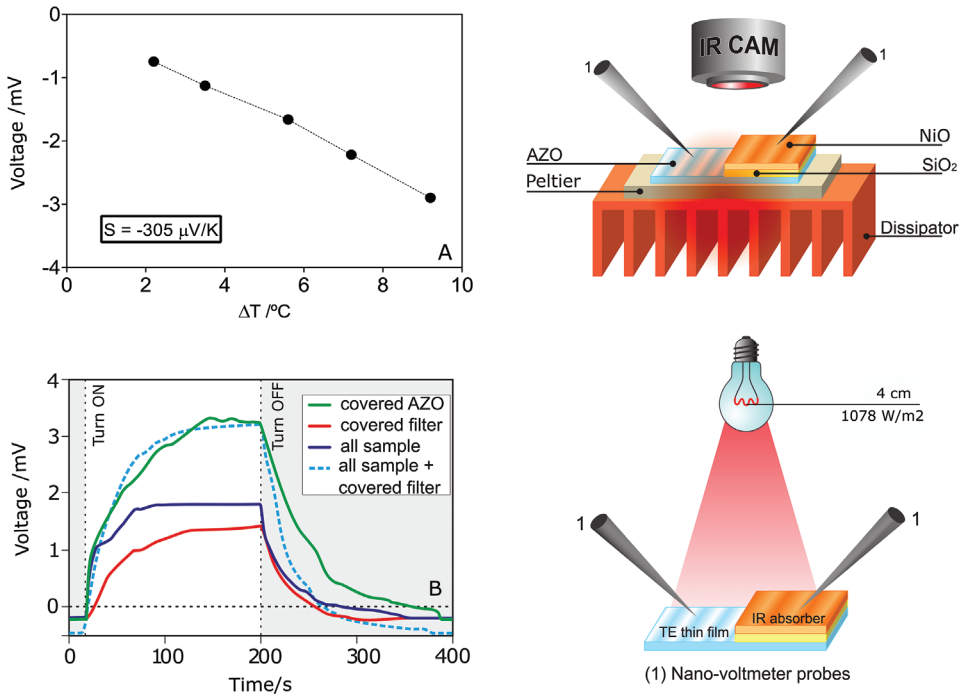

Figure 5. A) Potential versus temperature of TPTE and respective Seebeck coefficients and schematic of thermovoltage measurement (Blue layer—AZO thermoelectric thin film; Orange layer—SiO_2 + NiO layers, Red and blue (heating/cooling) heat sinks and Beige layer—Peltier module) and corresponding Seebeck coefficient and B) continuous monitoring of the voltage: covering different areas of the sample or irradiating the entire sample. Dashed line is the sum of voltage corresponding to the red (covered filter, i.e., radiating only AZO with IR light) and blue line (lighting the entire sample).

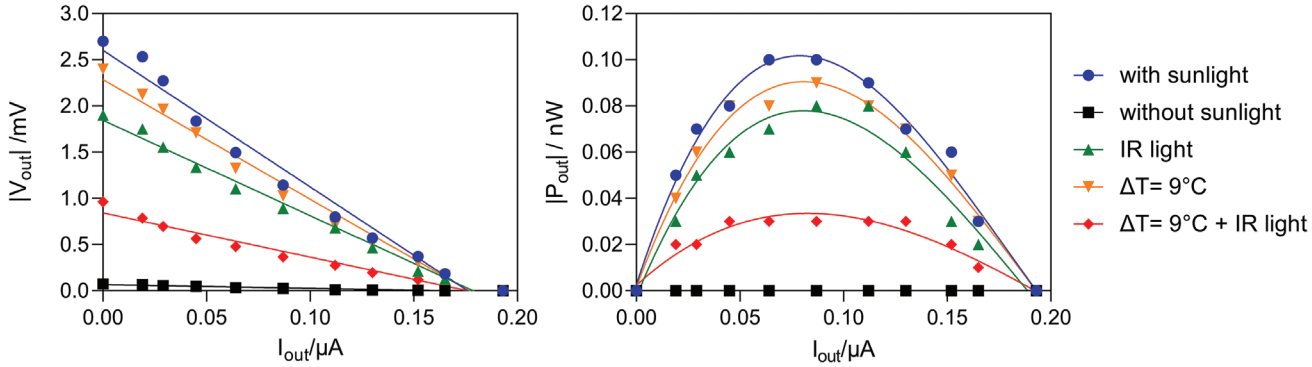

Figure 6. *I–V* curves measured in dark (black line), under sunlight (blue line), with a temperature gradient of 9 °C between AZO and NiO (orange line), under IR light (1078 W m^{-2}—green line) and temperature gradient plus IR light (red line).

The AZO/SiO_2/NiO structure was positioned in a single glass window facing south and the voltage and resistance (Figure S3, Supporting Information) were monitored over time. **Figure 7** displays voltage and solar irradiance intensity for two consecutive days and outlines a direct relationship between both. However, the SiO_2 layer thickness of AZO/SiO_2/NiO structure also plays an important role in the signal intensity. Since SiO_2 is an insulating material, it prevents the positive and negative charges formed on the electrodes from recombining. In this case, the potential obtained reflects the difference in the number of charges between the electrodes (AZO and NiO). However, if the SiO_2 layer is thin, it allows charge tunnelling between the electrodes, leading to a flow of carriers from one side of the junction to the other and the potential increases. Thus, the junction behaves as a tunnelling junction. The optimized structure (SiO_2 with 136 nm thick) was monitored for more than 5 months, covering summer and winter seasons (**Figure 8**). As compared to summer, the voltage signals increased for winter season, since temperature difference between outside 25 and inside building is superior (Figure S4, Supporting Information).

3. Conclusions

In this work a photothermoelectric effect in structures of AZO/SiO_2/NiO was demonstrated to be possible to obtain after annealing the NiO layer and optimizing its NIR absorption for values in the range of 40–50% for $\lambda > 700$ nm keeping transmittance in the visible wavelengths range within 40–60%. The

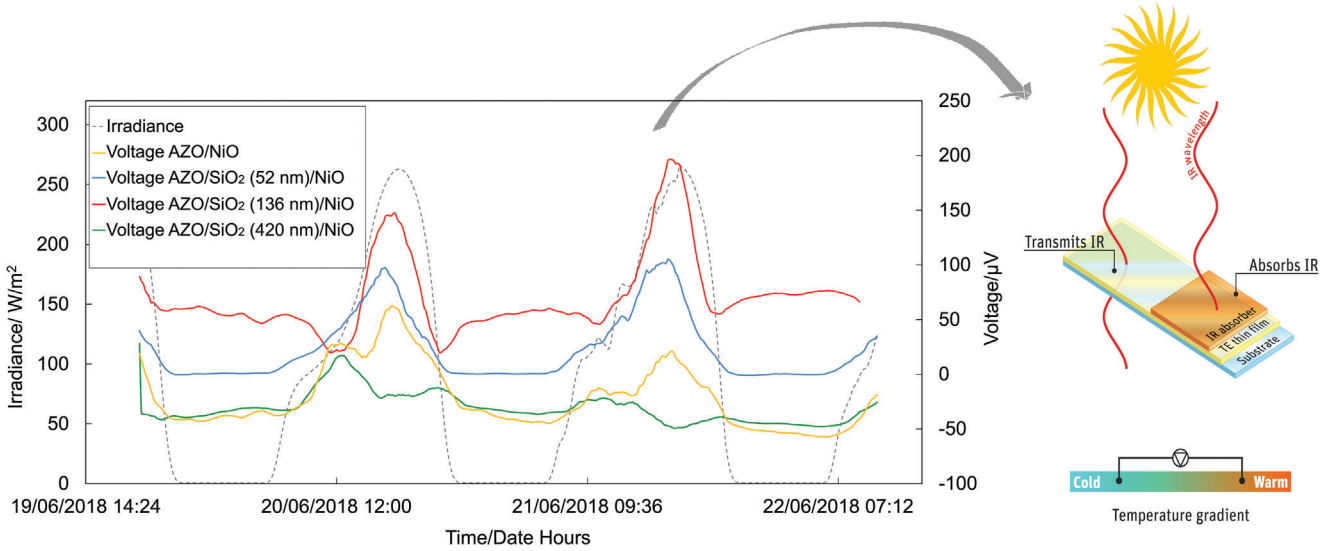

Figure 7. Voltage and Irradiance monitoring during 2 days of transparent photothermoelectric device with or without different thickness of SiO_2 layers glued to the window.

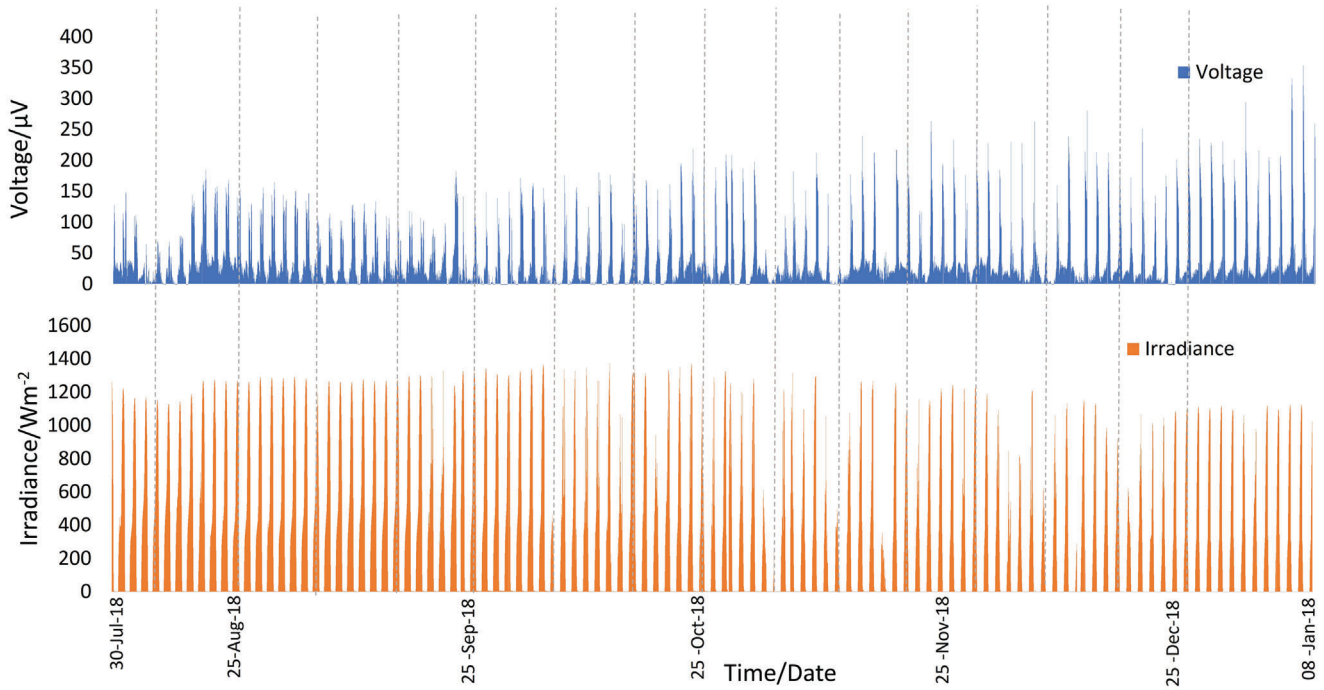

Figure 8. Voltage and Irradiance monitoring for 5 months (30th July to 8th January) of the transparent photothermoelectric device (AZO 90 nm/SiO_2 136 nm/50 nm of NiO layer, annealed at 500 °C during 1 h in vacuum conditions) glued to the window.

influence of SiO_2 layer thickness was studied to avoid charge recombination and it was concluded that the optimal thickness was 136 nm. A photothermal Seebeck of −0.3 mV K^{-1} was observed when irradiating the mentioned structure with infrared light. The voltage monitored over several weeks reveals its direct relation with solar radiation. Therefore, in this work a new concept of capturing NIR radiation and converting it into a voltage using transparent structures to visible light was demonstrated. These types of structures are particularly interesting for window glass applications.

4. Experimental Section

Film Deposition: The thermoelectric layer, aluminum-doped zinc oxide (AZO), was deposited by atomic layer deposition on glass substrate with 90 nm of thickness, following a procedure previously reported.[10]

The intermediate silicon dioxide (SiO_2) layer, was sputtered in a *Mantis* radio frequency (RF) magnetron sputtering at a working pressure around 9×10^{-4} mbar using an In:Sn alloy (90%:10%), 99.99% purity (supplied by Kurt J. Lesker Company) target. And it was undertaken under Argon atmosphere at a flow rate of 9.5 sccm and RF power of 250 W. Presputtering was performed for 10 min to remove the target surface contamination. The SiO_2 layer was deposited underneath.

NiO films with a thickness of 10, 30, or 50 nm were deposited by resistive thermal evaporation of NiO powders with 99.99% purity (supplied by GoodFellow, UK) in a tungsten boat at a pressure of 8×10^{-6} to 2×10^{-7} mbar. A postdeposition annealing was performed in a furnace (MTI Corporation—OTF-1200X-4-RTP) following a temperature-controlled ramp up of 30 min during 1 or 2 h at 500 and 600 °C, under vacuum pressure (2×10^{-4} mPa).

Film Characterization: The layers thickness was measured with a KLA Tencor D-600 Profilometer, and the optical properties of the multilayer thin film structures deposited on glass were accessed through the measurement transmittance, reflectance, and absorption spectra in the wavelength range from 200 to 2200 nm with a JASCO V-770 spectrophotometer. Samples compositional analysis was performed by confocal Raman spectroscopy in a Witec Alpha—300 RAS system, equipped with a 532 nm Argon Laser at 18 mW of power (each spectrum was acquired for 8 min). The surface topography and roughness of AZO and NiO films, before and after annealing, as well as the NiO top layer of the annealed multilayer structure were analyzed with the atomic force microscope of the WiTec Alpha 300 RAS confocal spectrometer. The cantilever was operated in tapping mode with an AFM probe with aluminum reflective coating at 75 kHz and a constant load of 2.8 N m^{-1}. Lateral and depth resolutions were 1 and 0.3 nm, respectively. Roughness was determined for all samples through maps root mean square height (Sq). For the Seebeck Coefficient calculation ($S = \Delta V/\Delta T$), the thermovoltage ΔV was measured with a nanovoltmeter (Agilent 34420A) as a function of the gradient temperature ΔT, *recorded* by an IR camera (FLIR A310) installed in a homemade apparatus.[12] A pair of aluminum electrodes were deposited on top of NiO and AZO films. The Seebeck measurements were performed with a transverse temperature gradient on the sample, i.e., the sample is uniformly heated and ΔV is measured in three different ways: two probes on AZO; two probes on NiO and between a probe placed on the AZO film electrode and another on the NiO electrode (schematized in Table S2, Supporting Information). This procedure was repeated to measure the photothermoelectric voltage signal of samples exposed to NIR light. The NIR lamp used, has an emission peak at 1000 nm wavelength and maximum intensity of 1078 Wm^{-2}.[26] The light radiated either the whole sample or only one side of the multilayer thin film structure (AZO or NiO side), depending on the part of the sample covered with a cork sheet. The photovoltage time response while switching the light ON and OFF was recorded in a computer controlled nanovoltmeter Agilent 34420A. Also, to ensure that there was no thermal gradient between contacts, the temperature over time was simultaneously monitored with the photovoltage. The open-circuit potential (V_{OC}) of the glass/AZO/SiO_2/NiO samples was measured by placing one probe on the AZO layer electrode and another on the NiO layer electrode, and it was continuously monitored on samples mounted in a south oriented window (where the top film was in contact with the inner glass of the window). Over several weeks, every 20 min, V_{OC} was recorded together with irradiance and temperature with a computer controlled datalogger (Keysight 34972A). A schematic of the complete readout system is shown in Figure S1 (Supporting Information).

Supporting Information

Supporting Information is available from the Wiley Online Library or from the author.

Acknowledgements

This work was mainly funded by ERC-CoG-2014, CapTherPV, 647596, and partially funded by FCT – Fundação para a Ciência e a Tecnologia, I.P., in the scope of the Project Nos. LA/P/0037/2020, UIDP/50025/2020, and UIDB/50025/2020 of the Associate Laboratory Institute of Nanostructures, Nanomodelling and Nanofabrication – i3N.

Conflict of Interest

The authors declare no conflict of interest.

Data Availability Statement

The data that support the findings of this study are available from the corresponding author upon reasonable request.

Keywords

infrared absorption, photothermoelectrics, transparent devices

Received: January 30, 2023
Revised: March 7, 2023
Published online:

[1] D. B. Patel, K. R. Chauhan, *J. Alloys Compd.* **2020**, *842*, 155594.
[2] M. Patel, H.-S. Kim, J. Kim, J.-H. Yun, S. J. Kim, E. H. Choi, H.-H. Park, *Sol. Energy Mater. Sol. Cells* **2017**, *170*, 246.
[3] K. Majhi, L. Bertoluzzi, K. J. Rietwyk, A. Ginsburg, D. A. Keller, P. Lopez-Varo, A. Y. Anderson, J. Bisquert, A. Zaban, *Adv. Mater. Interfaces* **2016**, *3*, 1500405.
[4] R. R. Lunt, V. Bulovic, *Appl. Phys. Lett.* **2011**, *98*, 113305.
[5] H. Kim, H.-S. Kim, J. Ha, N.-G. Park, S. Yoo, *Adv. Energy Mater.* **2016**, *6*, 1502466.
[6] J. Loureiro, N. Neves, R. Barros, T. Mateus, R. Santos, S. Filonovich, S. Reparaz, C. M. Sotomayor-Torres, F. Wyczisk, L. Divay, R. Martins, I. Ferreira, *J. Mater. Chem. A* **2014**, *2*, 6649.
[7] M. Ferreira, J. Loureiro, A. Nogueira, A. Rodrigues, R. Martins, I. Ferreira, *Mater. Today Proc.* **2015**, *2*, 647.
[8] J. Figueira, J. Loureiro, J. Marques, C. Bianchi, P. Duarte, M. Ruoho, I. Tittonen, I. Ferreira, *ACS Appl. Mater. Interfaces* **2017**, *9*, 6520.
[9] B. M. Morais Faustino, D. Gomes, J. Faria, T. Juntunen, G. Gaspar, C. Bianchi, A. Almeida, A. Marques, I. Tittonen, I. Ferreira, *Sci. Rep.* **2018**, *8*, 6867.
[10] A. C. Marques, J. Faria, P. Perdigão, B. M. M. Faustino, R. Ritasalo, K. Costabello, R. C. Da Silva, I. Ferreira, *Sci. Rep.* **2019**, *9*, 17919.
[11] J. Coroa, B. M. Morais Faustino, A. Marques, C. Bianchi, T. Koskinen, T. Juntunen, I. Tittonen, I. Ferreira, *RSC Adv.* **2019**, *9*, 35384.
[12] C. Bianchi, J. Loureiro, P. Duarte, J. Marques, J. Figueira, I. Ropio, I. Ferreira, *Adv. Mater. Technol.* **2016**, *1*, 1600077.
[13] C. Yang, D. Souchay, M. Kneiß, M. Bogner, H. M. Wei, M. Lorenz, O. Oeckler, G. Benstetter, Y. Q. Fu, M. Grundmann, *Nat. Commun.* **2017**, *8*, 16076.
[14] A. Tomeda, T. Ishibe, T. Taniguchi, R. Okuhata, K. Watanabe, Y. Nakamura, *Thin Solid Films* **2018**, *666*, 185.
[15] Y. Park, K. Cho, J. Choi, S. Kim, *J. Nanosci. Nanotechnol.* **2016**, *16*, 10563.
[16] N. Srinatha, Y. S. No, V. B. Kamble, S. Chakravarty, N. Suriyamurthy, B. Angadi, A. M. Umarji, W. K. Choi, *RSC Adv.* **2016**, *6*, 9779.
[17] B. Al Farsi, F. Al Marzouqi, M. Al-Maashani, M. T. Souier, M. Tay Zar Myint, M. Z. Al-Abri, *Mater. Sci. Eng. B* **2021**, *264*, 114977.
[18] F. J. Manjón, B. Marí, J. Serrano, A. H. Romero, *J. Appl. Phys.* **2005**, *97*, 053516.
[19] D. Liu, D. Li, D. Yang, *AIP Adv.* **2017**, *7*, 015028.
[20] W. J. Duan, S. H. Lu, Z. L. Wu, Y. S. Wang, *J. Phys. Chem. C* **2012**, *116*, 26043.

[21] W. Xiang, Y. Liu, J. Yao, R. Sun, *Phys. E* **2018**, *97*, 363.
[22] N. Mironova-Ulmane, A. Kuzmin, I. Sildos, L. Puust, J. Grabis, *Latv. J. Phys. Tech. Sci.* **2019**, *56*, 61.
[23] P. Ravikumar, B. Kisan, A. Perumal, *AIP Adv.* **2015**, *5*, 087116.
[24] S. Rakshit, S. Ghosh, S. Chall, S. S. Mati, S. P. Moulik, S. C. Bhattacharya, *RSC Adv.* **2013**, *3*, 19348.
[25] Standard Tables for References Solar Spectral Irradiance at Air Mass 1.5: Direct Normal and Hemispherical for a 37° Tilted Surface, http://www.astm.org/cgi-bin/resolver.cgi?G159-98 (accessed: **January 2021**).
[26] Incandescent reflector Infrared heat lamps /industrial, *Philips*, 38. https://joovv.com/blogs/joovv-blog/infrared-heat-lamps-vs-led-photobiomodulation-light-therapy-devices (accessed: January 2021).